LUMEN – DESIGN OF THE REGENERATIVE COOLING SYSTEM FOR AN EXPANDER BLEED CYCLE ENGINE USING METHANE

Jan Haemisch[(1)], **Dmitry Suslov**[(2)], **Günther Waxenegger-Wilfing**[(3)], **Kai Dresia**[(4)], **Michael Oschwald**[(5)]

[(1)-(5)] *Institute of Space Propulsion, DLR Lampoldshausen, Langer Grund, D-74239 Hardthausen, Jan.Haemisch@dlr.de, Dmitry.Suslov@dlr.de, Guenther.Waxenegger@dlr.de, Kai.Dresia@dlr.de, Michael.Oschwald@dlr.de*

KEYWORDS: LUMEN, HARCC, regenerative cooling, machine learning, design optimization

ABSTRACT

The regenerative cooling still is one of the most crucial parts in designing a liquid rocket engine. The goal of an effective design is a trade-off between a sufficient cooling of the structure and a low pressure drop in the cooling channels. For an expander type cycle a third requirement arises: A sufficient enthalpy increase of the cooling fluid for the turbopumps to operate effectively. To prevent the combustion chamber from melting, the regenerative cooling has to be designed with a sufficient margin to respect all uncertainties. A neural network based surrogate model is used to study the robustness of the cooling channel design for other load points of the engine.

In this paper, the design of the regenerative cooling system and the manufacturing of a subscale combustion chamber will be discussed.

NOMENCLATURE

α	heat transfer coefficient [$W/m/K$]
c_P	specific heat capacity at constant pressure [$J/kg/K$]
h	enthalpy [kJ/kg]
k_s	roughness [m]
L	combustion chamber length [mm]
$\dot{m}$	mass flow [kg/s]
n	number of cooling channels [-]
P	pressure [bar]
P_{cc}	combustion chamber pressure [bar]
P_{in}	inlet pressure [bar]
P_{out}	outlet pressure [bar]
ΔP	pressure drop [bar]
$\dot{q}_w$	wall heat flux [W/m^2]
T_{in}	fluid inlet temperature [K]
T_{out}	fluid outlet temperature [K]

1 INTRODUCTION

The regenerative cooling system for the LUMEN engine faces two major features: 1. Methane as coolant. 2. Usage of the coolant in an expander bleed system architecture. Methane has a much higher density, compared to hydrogen and can therefore be stored in smaller, lighter tanks. Due to the higher density the turbopumps demand significantly less power. Additionally insulation can be saved due to a higher boiling point. Major drawback is a reduction of the specific impuls. Nevertheless multiple LOX/CH_4 or LOX/LNG engines are currently under development [4, 16, 3].

Methane as coolant in regenerative cooling systems is a critical topic and a major concern for using methane as fuel for rocket engines. Methane has a higher density and a lower specific heat at constant pressure c_p, compared to hydrogen. The main different however is the vicinity to the critical point that may lead to *heat transfer deterioration* (HTD) [13, 15, 23].

The main goal of a common cooling channel design is to maximize the cooling efficiency in other words to reach the minimal hot gas side wall temperature with a minimal pressure loss. The lower the hot gas side wall temperature, the better the cooling performance since a temperature decrease of $dT = 40K$ doubles the engine life time [10]. For the cooling channel design of an expander-type engine a third goal arises: A sufficient increase of the coolant enthalpy to drive the turbopumps. This goal is in opposite to the maximal cooling since a large temperature increase of the coolant goes along a high wall temperature. The enthalpy increase of the coolant is the reason why expander-type engines typical display a long cylindrical combustion chamber part [1].

1.1 LUMEN Engine

THE LUMEN (Liquide Upper Stage deMonstator ENgine) is a Nozzle-Expander-Bleed (NEB) engine that uses methane as fuel and therefore also as coolant. The flow direction is *counterflow* for the nozzle and combustion chamber and *coflow* for the nozzle extension. Computational Fluid Dynamics

parameter	unit	value
T_{out}	$[K]$	> 400
T_w	$[K]$	< 900
$\Delta p_{channel}$	$[bar]$	< 25

Table 1: Goals for the cooling system design.

parameter	unit	value
cooling channel width	$[mm]$	≥ 1
width between cooling channels	$[mm]$	≥ 1
distance to hot gas side	$[mm]$	1
number of cooling channels	$[-]$	≤ 86

Table 2: Constraints due to manufacturing and structural reasons.

(CFD) is a commonly used tool for the calculation of heat transfer in cooling channels [26, 22, 15]. However most of the validation data is for hydrogen as cooling fluid. Data for methane as coolant is rare [12, 14, 27, 20]. In addition to that, the physical properties rapidly change in the vicinity of the critical point. These two points lead to significant deviations of the CFD simulations, especially close to the critical point [15]. This has to be kept in mind when discussing sufficient margin for the analysis.

The paper is divided into three parts: In the first part a method is described and used to find the optimal cooling channel geometry for an expander type engine. In the second part, a neural network model is presented and used to validate the found solution for different load points. The third part gives an overview of the manufacturing process of the subscale combustion chamber.

2 PART I: OPTIMIZATION OF COOLING CHANNEL GEOMETRY

Based on the boundary conditions and constrains, that are defined by a system analysis for the whole LUMEN engine, CFD simulations with varying geometry were performed to optimize the cooling channel geometry. An optimization algorithm is used to change the height, width and length of the cooling channels to find the solution that addresses all three goals: sufficient cooling, low pressure drop, large increase of coolant temperature.

2.1 goals for the design

The optimal design features a wall temperature below the allowed limit of 900K, an enthalpy increase of the coolant to get an outlet temperature of $T_{out} > 400\,K$, and the lowest pressure drop possible (at least $dP < 25\,bar$). The goals are summarized in Tab. 1. The constraints due to manufacturing reasons are summarized in Tab. 2.

These goals are not independent since a higher enthalpy increase would increase the turbopump performance and enlarge the allowed pressure drop. The other way around, a lower pressure drop could potentially allow a lower enthalpy increase. Since the turbopump is not part of the calculation, the goals are set to be fixed. In future versions of the calculation, the feedback of the turbomachinery might be added.

Due to manufacturing and structural reasons the width of the cooling channel is at least 1 mm and the distance between the cooling channels has to be at least 1 mm. The number of cooling channels is a consequence of these constraints in the nozzle throat. For the hot gas side wall temperature, the optimum is a constant temperature slightly below the temperature limit.

2.2 optimization parameters

To reach the goals with the given boundary conditions the geometry of the cooling channel can be varied. That includes the width and height along the cooling channel length, a varying length of the cylindrical part of the combustion chamber and the number of cooling channels. The nozzle geometry remains fixed. Despite the geometry, the coolant mass flow can be used as another parameter. The LUMEN system architecture allows to vary the mass flow for the cooling channels within a certain range. The roughness is assumed to be constant.

Due to simplification and manufacturing reasons, the cooling channel geometry can be changed at 5 characteristic positions along the combustion chamber length. In between the values are interpolated linearly. Fig. 1 shows the positions depending on the assumed heat flux profile. The characteristic positions are the begin and end of the decreasing heat flux in the cylindrical part, the nozzle and the beginning and end of the combustion chamber. Additionally the length of the cylindrical part (between h2 and h3) can be varied.

2.3 Boundary conditions

The main boundary conditions for the cooling channel design are the assumed heat flux profile, the maximal mass flow and the assumed roughness in the channels.

The LUMEN engine is designed to work for load points between a combustion chamber pressure between $P_{cc} = 35\,bar$ and $P_{cc} = 80\,bar$ and the mixture ratio (ROF) between 3 and 3.8.

The geometry optimization will be performed for the nominal point, that is: $P_{cc} = 60\,bar$ and $ROF = 3.4$. The boundary conditions for the CFD simulation for this load point can be found in Tab. 3. When a solution for this load point is found, the performance for the other load points will be verified.

The heat flux profile is the result of a ROCFLAM III simulation [19, 21].

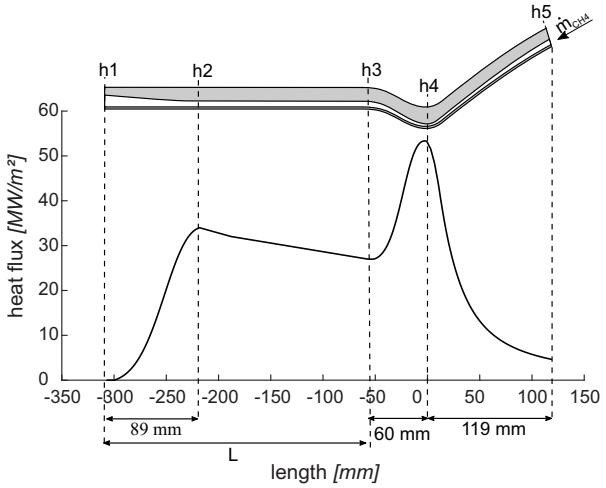

Figure 1: Positions at which the cooling channel geometry is optimized.

parameter	unit	value
$\dot{q}_w$	$[MW/m^2]$	Fig. 2
T_{ein}	$[K]$	120
P_{out}	$[bar]$	68.4
k_s	$[m]$	5e-6
$\dot{m}_{CH_4}$	$[kg/s]$	< 2.8

Table 3: Boundary conditions for the CFD simulations.

The profile that is shown in Fig. 2 was calculated for a fixed combustion chamber contour, however it was adapted to use it for different lenghts of the cylindrical part of the combustion chamber. The first peak after the injector head and the slope of the decreasing heat flux is held constant. This leads to a lower heat flux at the beginning of the nozzle part for a longer cylindrical part. The overall heat flux is of course larger for a longer combustion chamber. The heat flux in the nozzle and nozzle extension is assumed to be independent from the combustion chamber length.

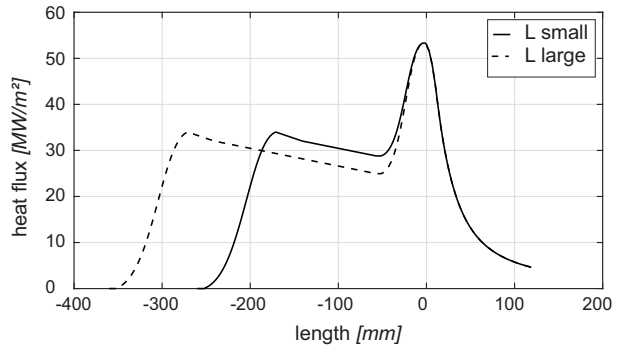

Figure 2: Assumed heat flux profile $\dot{q}_w$ for different lengths of the cylindrical part of the combustion chamber L.

parameter	unit	value
L	$[mm]$	247.2
h1	$[mm]$	8.2
h2	$[mm]$	4.0
h3	$[mm]$	4.0
h4	$[mm]$	1.8
h5	$[mm]$	4.1
$n_{channel}$	$[-]$	86
$\dot{m}_{CH_4}$	$[-]$	2.35

Table 4: Geometry parameter for the final design.

2.4 The numerical setup

RANS simulations were performed with the commercial software ANSYS CFX [2]. The SST turbulence model was used. The used mesh is adapted to each iteration step so that the cell width and heights remain constant to get comparable results. The the y+-value is <1. More details for the numerical setup can also be found in [15].

2.4.1 optimization procedure

As optimization scheme the Multi-Objective Generic Algorithm (MOGA) algorithm is used [9]. The width and heights are changed after each step and a CFD calculation was performed.

3 RESULTS

In this section, the results of the optimization will be discussed. Two different approaches were analyzed: At first, a constant distance between the cooling channels was assumed. This approach leads to smaller channels in the nozzle part, where the heat load is higher and wider channels in the nozzle extension where heat load is lower. This should lead to a better cooling where it is necessary and a low pressure drop where the cooling demand is less relevant. However the results were insufficient and no solution was found that fulfills all three goals. The approach was changed to a constant cooling channel width of $1\,mm$. This approach improved the results significantly and led to the final cooling channel geometry.

3.1 constant cooling channel width

A constant cooling channel width is comparatively much easier to manufacture, and the results show that also the cooling performance is enhanced compared to the constant distance between cooling channels approach. This is due to a higher aspect ratio (height-to-width-ratio) compared to the case with constant distance between the cooling channels.This enhances the cooling performance and also lowers the risk of the occurrence of heat transfer deterioration [13, 17].

parameter	unit	value
T_{out}	$[K]$	408.6
$T_{w_{h2}}$	$[K]$	874.1
$T_{w_{h4}}$	$[K]$	879.1
$\Delta p_{channel}$	$[bar]$	23.7

Table 5: Results for the CFD simulation of the final design.

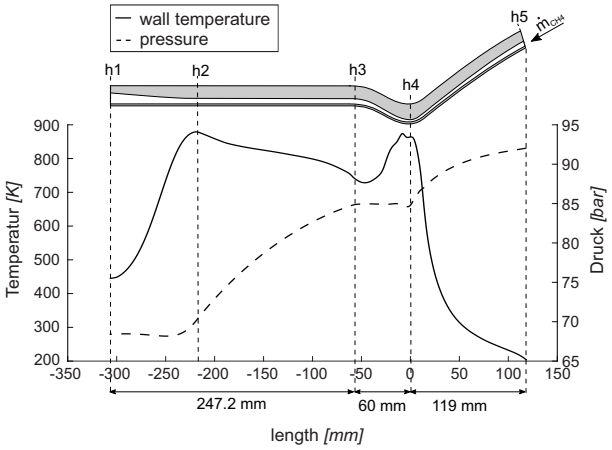

Figure 3: Temperature and pressure distribution for the optimized designpoint.

The drawback is a larger distance between the cooling channels. However due to a wall material with a high thermal conductivity and low heat flux in the nozzle extension the cooling performance can still be enhanced.

After almost 500 CFD Simulations, an optimized solution was found. Fig. 3 shows the Temperature and pressure distribution for the final cooling channel geometry. The final geometric parameter are summarized in Tab. 4 and the results for the final CFD simulation in Tab. 5 and Fig. 4. The design fulfills all requirements that were defined in Tab. 1.

The hot gas side wall temperature distribution shows two peaks at positions h2 and h4 that correlate with the peaks of heat flux profile (Fig. 2).

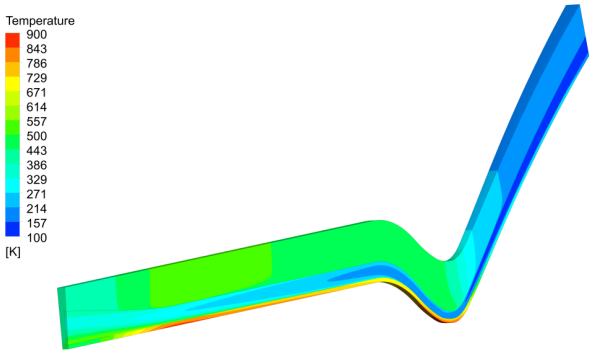

Figure 4: Temperature distribution for the optimized designpoint.

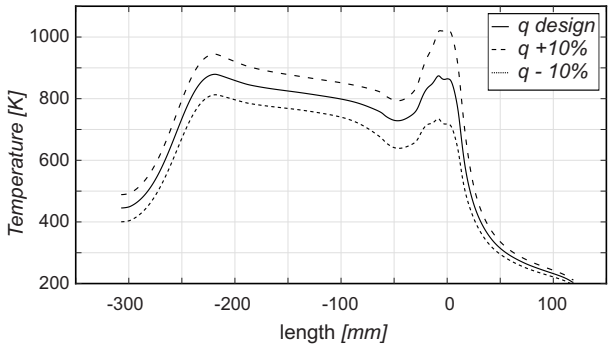

(a) heat flux

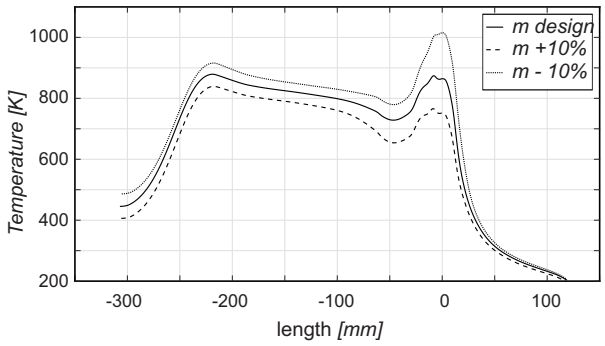

(b) massflow

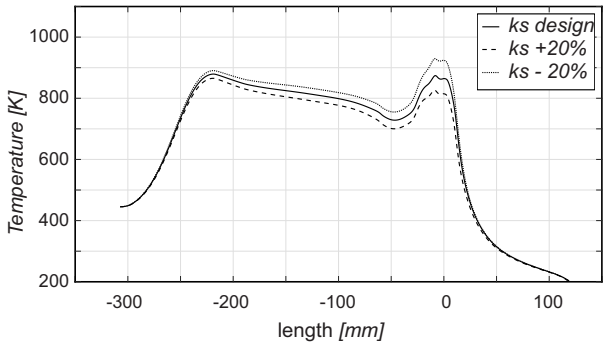

(c) roughness

Figure 5: Influence of uncertainties to the hot gas side wall temperature.

Although the heat flux peak at h2 is significant lower both peaks show a comparable high temperature of about $T_w \approx 880K$. This distribution is in accordance with the optimal temperature distribution, defined in section 2.1 (a constant temperature slightly below the temperature limit) and leads to a minimal pressure drop.

The length of the cylindrical part is enlarged by almost $50\,mm$ compared to the initial design. Due to the additional heat flux, the outlet temperature T_{out} was maximized.

3.2 impact of uncertainties

To check how the results change due to uncertainties of the boundary conditions, simulations were performed with $\pm 10\%$ to the assumed value. It was analyzed: Heat flux distribution, $\dot{q}_w$, massflow, $\dot{m}$, and roughness, k_s. Fig. 5 shows the results for

these simulations. It can be seen that the highest deviations occur close to the nozzle throat. For the design point, two peaks in the hot gas side wall temperature occur. For deviations in heat flux ($\dot{q}_w + 10\%$) or mass flow ($\dot{m} - 10\%$) the peak close to the nozzle throat is significant higher. On the other hand the peak at $-250\,mm$ is higher for the deviations with changing signs ($\dot{q}_w - 10\,\%$; $\dot{m} + 10\,\%$). The optimum is only valid for the design point. Deviations in roughness ($k_s \pm 20\,\%$) only play a minor role.

4 PART II: NEURAL NETWORK BASED SURROGATE MODEL FOR THE MAXIMUM WALL TEMPERATURE

The main disadvantage of CFD simulations is that they are not suitable for design space exploration and extensive sensitivity analysis due to their large calculation effort. By constructing surrogate models using samples of the computationally expensive calculation, one can alleviate this burden. However, it is crucial that the surrogate model mimics the behavior of the simulation model as closely as possible and generalizes well to unsampled locations, while being computationally cheap to evaluate. Neural networks (NNs) are known to be universal function approximators [11] and have been successfully applied as surrogate models in many domains, including avionics [24, 8] and space [7, 18].

To overcome the low accuracy of empirical heat-transfer correlations for methane, Waxenegger-Wilfing et al. [29] developed an NN-based surrogate model to predict the maximum wall temperature along the cooling channel of the combustion chamber. Trained with data from full three-dimensional CFD simulations, the model achieves high accuracy and can predict the maximum wall temperature even close to the critical point. The NN uses a fully connected, feedforward architecture with 4 hidden layers and 408 neurons per layer.

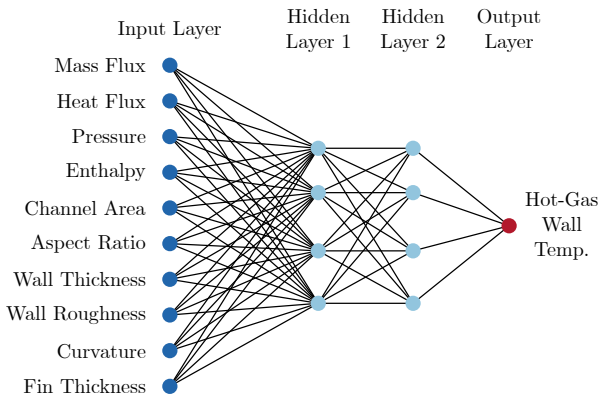

Figure 6: Exemplary NN architecture.

4.1 Comparison NN with CFD

After training, the NN can predict the maximum wall temperature for previously unseen test cases, including different channel geometries and operation conditions. For the subsequent results, the model was extended for different channel curvatures and rib thicknesses. Figure 6 shows an exemplary architecture with two hidden layers, four neurons per hidden layer, and all input parameters. The NN is combined with further reduced-order models that calculate the stream-wise development of the coolant pressure and enthalpy. Thus, predictions with a precision similar to full CFD calculations are possible. The prediction of an entire channel segment takes only 0.6 s, which is at least 1000 times faster than comparable three-dimensional CFD simulations.

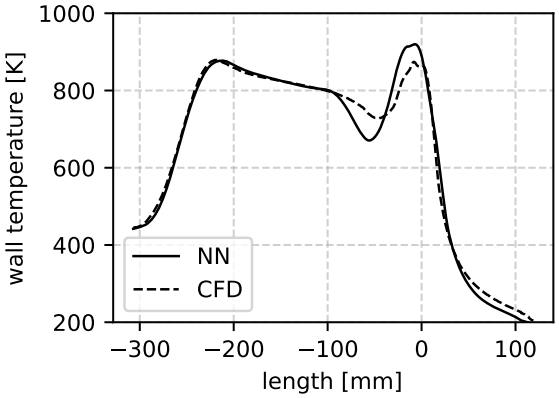

Figure 7: Comparison between CFD and NN-based calculations for a combustion chamber pressure of 60 bar*.*

parameter	unit	CFD	NN
T_{out}	[K]	408.6	409.1
$\Delta p_{channel}$	[bar]	23.7	20.4
$T_{w_{h2}}$	[K]	874.1	920.0
$T_{w_{h4}}$	[K]	879.1	877.2

Table 6: Comparison between CFD and NN-based calculations for a combustion chamber pressure of 60 bar*.*

Figure 7 and Table 6 compare the predictions of the NN with CFD results for a combustion chamber pressure of 60 bar. Figure 7 shows that the NN captures the wall temperature curve very well, especially in the cylindrical segment. Deviations downstream of the nozzle throat ($length < 0\,\text{mm}$) are caused by inertia effects, which are not taken into account. Studies are currently underway to determine how these effects can also be included in the NN. As Table 6 indicates, the full surrogate model matches the outlet temperature very well (conservation of energy), but the pressure drop is slightly underestimated.

4.2 Results for 30 and 85 bar

The NN-based surrogate model is now used to study the cooling channel performance for other loads points of the LUMEN engine, i.e. a combustion chamber pressure of 35 bar and 80 bar. Table 7 shows the boundary conditions, where α is the scaling factor to adjust the heat flux profile to different combustion chamber pressures. α is calculated under the assumption that the heat flux scales with an exponent of 0.8 with respect to the chamber pressure [25]. The mass flow rate $\dot{m}$ and the cooling channel outlet pressure p_{out} are varied to study their implications on the wall temperature. Typical values were chosen based on the last iteration of the LUMEN cycle analysis.

parameter	unit	35 bar	80 bar
T_{in}	[K]	120	120
α	$[-]$	0.65	1.26
p_{out}	[bar]	50-95	90-135
$\dot{m}$	$[\mathrm{kg\,s^{-1}}]$	1.4-2.0	3.4-4.0

Table 7: Boundary conditions for a combustion chamber pressure of 35 bar *and* 80 bar*, respectively.*

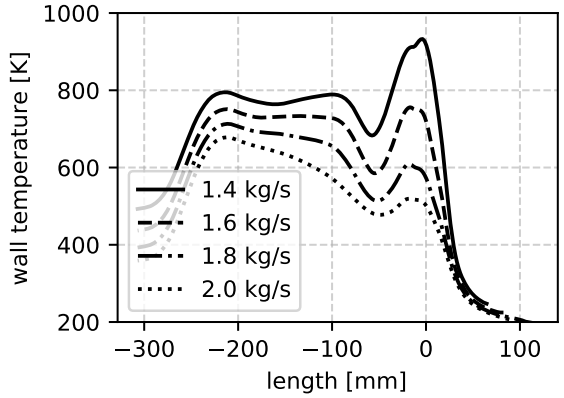

Figure 8: Wall temperature for a combustion chamber pressure of 35 bar *and a cooling channel outlet pressure of* 80 bar*.*

Figure 8 and Figure 9 show the result for a chamber pressure of 35 bar and 80 bar and a fixed cooling channel outlet pressure. For the given cooling channel geometry, the wall temperature maximum is either close to the nozzle throat or in the cylindrical part of the chamber. For higher coolant mass flows, the maximum is in the cylindrical part, whereas the wall temperature for lower mass flows rises sharply close to the nozzle throat. In the 80 bar case the temperature maximum is always in the cylindrical part whereas in the 35 bar case both situations can occur and transcritical effects play an essential role. Overall, the cooling channel design can achieve maximum wall temperatures below 850 K for both operating conditions and realistic coolant mass flows.

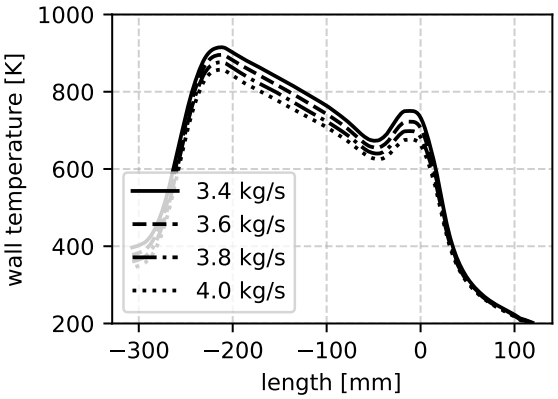

Figure 9: Wall temperature for a combustion chamber pressure of 80 bar *and a cooling channel outlet pressure of* 105 bar*.*

It is also interesting to study the pressure dependency of the results. Figure 10 and Figure 11 show the maximum wall temperature for given coolant mass flow and cooling channel outlet pressure. As already mentioned, the maximum wall temperature for small coolant mass flows and 35 bar combustion chamber pressure is close to the nozzle throat. The temperature maximum decreases with higher pressure because transcritical effects and the influence of HTD become weaker. The drop is followed by a horizontal evolution. This is due to the fact that the maximum wall temperature then appears close to the injector, where the coolant is supercritical and no significant pressure dependence is present. The same applies to the 80 bar case.

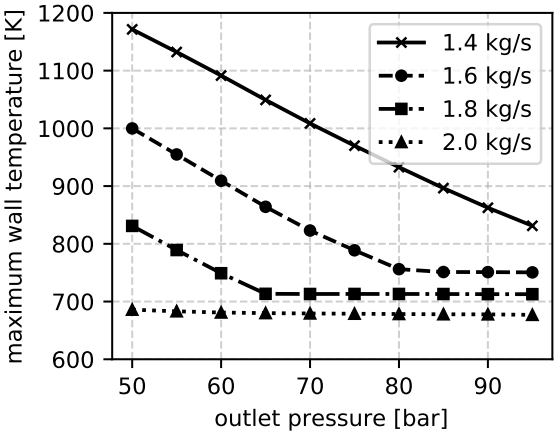

Figure 10: Pressure dependency of the maximum wall temperature for 35 bar*.*

In the LUMEN project, a maximum pressure drop in the cooling channel was specified. In the future, it might be interesting to include other elements in the design process, such as the turbopumps, additive manufacturing, fatigue life expectations of the combustion chamber [28], or control aspects [6]. Here,

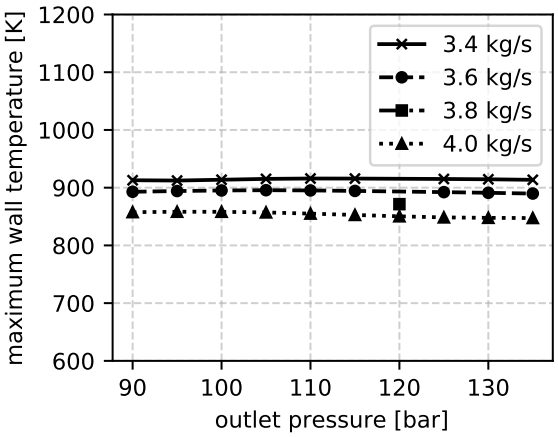

Figure 11: Pressure dependency of the maximum wall temperature for 80 bar.

an NN-based wall temperature prediction is an appealing alternative. Finally, it might also be possible to design an entire engine or launch vehicle in a global multidisciplinary design process to lower the expected costs [5].

5 PART III: MANUFACTURING OF THE COMBUSTION CHAMBER

The following steps were performed to build the combustion chamber:

1. turning of the first outer contour
2. milling of the cooling channels and drilling of holes for measurement technique
3. filling the cooling channels with wax and closing with electro deposit copper (3 layers). After each layer: drilling of holes for measurement technique and openings for the inlet and outlet manifolds.
4. turning of the final outer contour
5. turning of the final inner contour

5.1 Timeframe

From the beginning of the manufacturing (freezing CAD model and drawings) until the delivery of the final combustion chamber it took nearly 18 months. It took some effort to mill the cooling channels to the high accuracy that is necessary to gain reliable results in the test campaigns. However the by far longest time took the electro deposit of the copper jacket (>12 months). Due to the technical specifics It is not possible to accelerate this manufacturing step.

Alternatives that have to be analyzed to solve this problem are for example the manufacturing with SLM techniques.

(a) Picture of the manufacturing process. Combustion chamber after step 2.

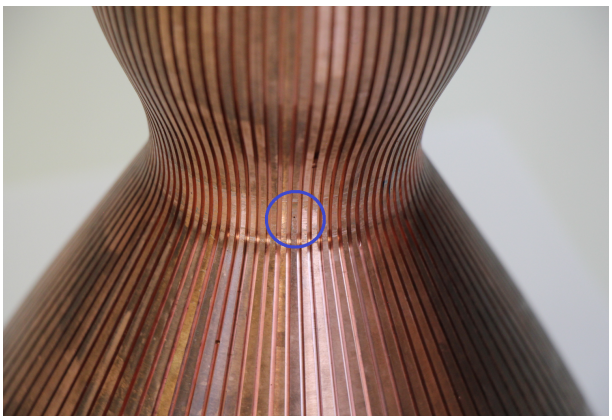

(b) Picture of the manufacturing process. Detail of the nozzle throat with measurement holes ($\varnothing = 0.25\,mm$) after step 2.

(c) Picture of the manufacturing process. Detail of the nozzle with openings for the manifold after the firs electro deposit layers.

(d) Picture of the manufacturing process. Combustion chamber after step 4 with final outer contour (without manifolds).

Figure 12: Pictures of the manufacturing process

6 CONCLUSION

In this paper the regenerative cooling system for an expander bleed-type engine was optimized. CFD simulations were used to calculate the cooling channel performance and to optimize the cooling channel geometry. An optimized solution was found that ensures sufficient cooling, sufficient enthalpy increase and a minimal pressure drop.

The performance of the cooling system was validated for all load points with a neural network model that significantly reduces the computational effort compared with CFD simulations.

The manufacturing of the combustion chamber is nearly completed and the tests for the finalized combustion chamber are scheduled for this year.

To reduce uncertainties and to prepare future simulations, the cooling channels are extensively measured during the manufacturing process. That includes roughness measurements at the side and bottom part of the channels. This knowledge in addition to hot fire tests will help to design an even more efficient cooling channel design in the future.

7 ACKNOWLEDGEMENTS

The authors would like to thank Sebastian Schulze who prepared the optimization scheme and performed the simulations, Andreas Märklen who is responsible for the combustion chamber manufacturing and ArianeGroup in Ottobrunn who performed the hot gas simulations for the heat flux boundary condition.

REFERENCES

[1] Alliot, P. : The VINCI upper stage engine: toward the demonstration of maturity. In: *AIAA 2013-4054, 49 th AIAA/ASME/SAE/ASEE Joint Propulsion Conference and Exhibit July 2013, San Jose, California*, 2013

[2] ANSYS: *Theory Guide, 18.0*

[3] Asakawa, H. ; Nanri, H. ; Aoki, K. ; Kubota, I. ; Mori, H. ; Ishikawa, Y. ; Kimoto, K. ; Ishihara, S. ; Ishizaki, S. : The Status of the Research and Development of LNG Rocket Engines in Japan. In: *Springer Aerospace Technology, Chemical Rocket Propulsion: A Comprehesive Survey of Energetic Materials*. – doi: 10.1007/978–3–319–27748–6–19, 2017

[4] Börner, M. ; Manfletti, C. ; Hardi, J. ; Suslov, D. ; Kroupa, G. ; Oschwald, M. : Laser ignition of a multi-injector LOX/methane combustor. In: *CEAS Space Journal, 10:273-286*. – doi: 10.1007/s12567–018–0196–6, 2018

[5] Dresia, K. ; Jentzsch, S. ; Waxenegger-Wilfing, G. ; Hahn, R. ; Deeken, J. ; Oschwald, M.

; Mota, F. : Multidisciplinary Design Optimization of Reusable Launch Vehicles for Different Propellants and Objectives. In: *AIAA Journal of Spacecraft and Rockets*. – doi: 10.2514/1.A34944, 2021

[6] Dresia, K. ; Waxenegger-Wilfing, G. ; Deeken, J. ; Oschwald, M. : Nonlinear Control of an Expander-Bleed Rocket Engine Using Reinforcement Learning. In: *Proceedings of the Space Propulsion 2020+1 Conference*. Virtual Event, 2021

[7] Dresia, K. ; Waxenegger-Wilfing, G. ; Riccius, J. ; Deeken, J. ; Oschwald, M. : Numerically Efficient Fatigue Life Prediction of Rocket Combustion Chambers Using Artificial Neural Networks. In: *Proceedings of the 8th European Conference for Aeronautics and Space Sciences (EUCASS)*. Madrid, Spain, 2019

[8] EASA: *Artificial Intelligence Roadmap - A Human-Centric Approach to AI in Aviation*. 2020

[9] Fonseca, C. M.: Genetic Algorithms for Multiobjective Optimization: Formulation, Discussion and Generalization. In: *Genetic Algorithms: Proceedings of the Fifth International Conference (S. Forrest, ed.), San Mateo, CA: Morgan Kaufmann, July 1993*, 1993

[10] Fröhlich, A. ; Popp, M. ; Schmidt, G. ; Thelemann, D. : Heat Transfer Characteristics of H2/O2 - Combustion Chambers. In: *AIAA/SAE/ASME/ASEE 29th Joint Propulsion Conference June 28-30, 1993 / Monterey, CA*. – doi: 10.2514/6.1993–1826, 1993

[11] Goodfellow, I. ; Bengio, Y. ; Courville, A. : *Deep Learning*. Cambridge, Massachusetts : The MIT Press, 2016 (Adaptive Computation and Machine Learning). – ISBN 978–0–262–03561–3

[12] Haemisch, J. ; Suslov, D. ; Oschwald, M. : Experimental Analysis of Heat Transfer Processes in Cooling Channels of a Subscale Combustion Chamber at Real Thermal Conditions for Cryogenic Hydrogen and Methane. In: *6th Space Propulsion Conference, 14-18th May 2018, Sevilla*, 2018

[13] Haemisch, J. ; Suslov, D. ; Oschwald, M. : Experimental study of Methane Heat Transfer Deterioration in a Subscale Combustion Chamber. In: *Journal of Propulsion and Power*. – doi: 10.2514/1.B37394, 2019

[14] Haemisch, J. ; Suslov, D. ; Oschwald, M. : Experimental Investigations of Heat Transfer Processes in Cooling Channels for Cryogenic Hydrogen and Methane at Supercritical Pressure. In: *In book: Non-Ideal Compressible Fluid Dynamics for Propulsion and Power*. – doi: 10.1007/978–3–030–49626–5, 2020

[15] Haemisch, J. ; Suslov, D. ; Oschwald, M. : Experimental and Numerical Investigation of Heat Transfer Processes in Rocket Engine Cooling Channels Operated with Cryogenic Hydrogen and Methane at Supercritical Conditions. In: *Transactions of the Japan Society for Aeronautical and Space Sciences, Aerospace Technology Japan 19(1):96-105*. – doi: 10.2322/tastj.19.96, 2021

[16] Kato, T. ; Terakado, D. ; Nanri, H. ; Morito, T. ; Masuda, I. ; Asakawa, H. ; Sakaguchi, H. ; Ishikawa, Y. ; Inoue, T. ; Ishihara, S. ; Sasaki, M. : Subscale Firing Test for Regenerative Cooling LOX/Methane Rocket Engine. In: *7th European Conference for Aeronautics and Space Science (EUCASS)*, 2017

[17] Leonardi, M. ; Pizzarelli, M. ; Nasuti, F. : Analysis of thermal stratification impact on the design of cooling channels for liquid rocket engines. In: *International Journal of Heat and Mass Transfer 135 (2019) 811-821*. – doi: 10.1016/j.ijheatmasstransfer.2019.02.028, 2019

[18] Ma, H. ; Zhang, Y.-x. ; Haidn, O. J. ; Thuerey, N. ; Hu, X.-y. : Supervised Learning Mixing Characteristics of Film Cooling in a Rocket Combustor Using Convolutional Neural Networks. In: *Acta Astronautica*. – doi: 10.1016/j.actaastro.2020.05.021, Okt. 2020. – ISSN 0094–5765

[19] M.Frey ; B.Kniesner ; O.Knab: Consideration of Real Gas Effects and Condensation in a Spray Combustion Rocket Thrust Chamber Design Tool. In: *3rd European Conference for Aerospace Sciences, Versailles, Frabce, 6-9 July 2009, EUCASS2009-85*, 2009

[20] Negishi, H. ; Daimon, Y. ; Kawashima, H. ; Yamanashi, N. : Flowfield and Heat Transfer Characteristics of Cooling Channel Flows in a Methane-Cooled Thrust Chamber. In: *48th AIAA/ASME/SAE/ASEE Joint Propulsion Conference & Exhibit 30 July - 1 August 2012, Atlanta, Georgia*. – doi: 10.2514/6.2012–4122, 2012

[21] O.Knab ; M.Frey ; J.Görgen ; C.Maeding ; K.Quering ; D.Wiedmann: Progress in Combustion and Heat Transfer Modelling in Rocket Thrust Chamber Applied Engineering. In: *45th AIAA/ASME/SAE/ASEE Joint Propulsion Conference & Exhibit 2 - 5 August 2009, Denver, Colorado, AIAA 2009-5477*. – doi: 10.2514/6.2009–5477, 2009

[22] Pizzarelli, M. : A CFD-derived Correlation for Methane Heat Transfer Deterioration. In: *Numerical Heat Transfer, Part A 2016, Vol.69, No. 3, 242-264*. – doi: 10.1080/10407782.2015.1080575, 2016

[23] Pizzarelli, M. : The status of the research on the heat transfer deterioration in supercritical fluids: A review. In: *International Communications in Heat and Mass Transfer, Volume 95, July 2018, Pages 132-138*. – doi: 10.1016/j.icheatmasstransfer.2018.04.006, 2018

[24] Sun, G. ; Wang, S. : A Review of the Artificial Neural Network Surrogate Modeling in Aerodynamic Design. In: *Proceedings of the Institution of Mechanical Engineers, Part G: Journal of Aerospace Engineering*. – doi: 10.1177/0954410019864485, Dez. 2019. – ISSN 0954–4100

[25] Sutton, G. P. ; Biblarz, O. : *Rocket Propulsion Elements*. 7th ed. New York : John Wiley & Sons, 2001. – ISBN 978–0–471–32642–7

[26] Urbano, A. ; Nasuti, F. : Onset of Heat Transfer Deterioration in Supercritical Methane Flow Channels. In: *Journal of Thermophysics and Heat Transfer Vol. 27, No. 2, April-June*. – doi: 10.2514/1.T4001, 2013

[27] Votta, R. ; Battista, F. ; Salvatore, V. ; Pizzarelli, M. ; Leccese, G. ; Nasuti, F. ; Meyer, S. : Experimental investigation of transcritical methane flow in rocket engine cooling channel. In: *Applied Thermal Engineering, Volume 101, 25 May 2016, Pages 61-70*. – doi: 10.1016/j.applthermaleng.2015.12.019, 2016

[28] Waxenegger, G. ; Riccius, J. ; Zametaev, E. ; Deeken, J. ; Sand, J. : Implications of Cycle Variants, Propellant Combinations and Operating Regimes on Fatigue Life Expectancies of Liquid Rocket Engines. 2017

[29] Waxenegger-Wilfing, G. ; Dresia, K. ; Deeken, J. C. ; Oschwald, M. : Heat Transfer Prediction for Methane in Regenerative Cooling Channels with Neural Networks. In: *Journal of Thermophysics and Heat Transfer*. – doi: 10.2514/1.T5865, 2020. – ISSN 1533–6808